Available online at www.sciencedirect.com
ScienceDirect
Earth and Planetary Science Letters 253 (2007) 282–290
EPSL
www.elsevier.com/locate/epsl

Electronic spin transitions in iron-bearing $MgSiO_3$ perovskite

Stephen Stackhouse *, John P. Brodholt, G. David Price

Department of Earth Sciences, University College London, Gower Street, London WC1E 6BT, UK

Received 17 July 2006; received in revised form 16 October 2006; accepted 17 October 2006
Available online 1 December 2006
Editor: R.D. van der Hilst

Abstract

The electronic spin state of iron in perovskites with the chemical composition $Mg_{0.9375}Fe_{0.0625}SiO_3$, $Mg_{0.8750}Fe_{0.1250}SiO_3$ and $Mg_{0.9375}Fe_{0.0625}Si_{0.9375}Fe_{0.0625}O_3$, have been determined at 0 K and various pressures between 40–160 GPa, using *ab initio* methods. The results indicate that ferric iron exhibits a wide range of spin transition pressures between about 60–160 GPa, while ferrous iron has a much narrower span, between about 130–145 GPa. In general, the lowest spin transition pressures are associated with the most energetically favorable substitution configurations, where iron atoms are closest together. The effect of spin state on calculated elastic properties is found to be small.

Keywords: ab initio; iron; perovskite; spin transitions; elastic properties; lower mantle

1. Introduction

The lower mantle is believed to be predominantly composed of iron-bearing magnesium silicate perovskite, coexisting with small amounts of magnesiowüstite and calcium silicate perovskite [1], which transforms to post-perovskite in the lowermost few hundred kilometers [2]. In addition, 5–20 km thick ultra-low velocity regions [3], postulated to comprise an iron-rich phase [4–6], are observed, in places, at the core–mantle boundary. In order to interpret seismic data and construct geophysical models of the lower mantle it is essential to have a detailed knowledge of the physical and chemical properties of these iron-containing phases.

Previous theoretical studies have examined the effect of incorporating ferrous [7] and ferric [8] iron on the elastic and seismic properties of magnesium silicate perovskite, under lower mantle pressures. These report that the presence of ferrous or ferric iron, in the amounts expected in the lower mantle, causes a decrease in longitudinal and shear isotropic wave velocities of about 1 and 2%. In the case of ferric iron [8] the influence of the spin state of iron on the elastic properties was also investigated and found to be negligible. This is surprising in light of recent experimental work showing the spin state of iron in magnesiowüstite to have a sizeable effect on its bulk modulus [9]. It is possible that the effect may be more pronounced for ferrous iron than ferric, however, the degree to which the spin state of ferrous iron in perovskite affects its elastic and seismic properties remains unknown.

It has recently been shown that iron in perovskite undergoes a high to low-spin transition under pressures corresponding to those of the lower mantle [10,11]. If a

* Corresponding author. Tel.: +44 20 7679 3424; fax: +44 20 7679 2685.
E-mail addresses: s.stackhouse@ucl.ac.uk (S. Stackhouse), j.brodholt@ucl.ac.uk (J.P. Brodholt), d.price@ucl.ac.uk (G.D. Price).

0012-821X/$ - see front matter © 2006 Elsevier B.V. All rights reserved.
doi:10.1016/j.epsl.2006.10.035

large contrast exists in the physical properties of perovskite containing iron in a high and low-spin state, such a transition could, depending on its sharpness, result in a seismic velocity discontinuity at the related depth. Further geophysical implications of such a spin transition in the lower mantle also exist. In the first instance, because the spin state of iron influences its ionic radius, it could affect partitioning, leading to compositional layering [10,12]. It has also been postulated that the spin state of iron in lower mantle minerals influences thermal conductivity, and could, therefore, have a significant effect on mantle convection [10,13]. The exact mechanism of spin transitions of iron in perovskite is, however, still unclear, with some reporting a gradual decrease in spin [11,14], and others reporting that two distinct spin transitions are observed [10]. More detailed experimental investigations [15] and recent theoretical calculations [16] have connected the first of the two spin transitions to ferric iron, while the second has been postulated to be associated with ferrous iron [17]. Extrapolation of these results to lower mantle temperatures, by means of calculations based on simple thermodynamic relationships combined with crystal field theory [18], suggests that high to low-spin transitions may not occur in ferrous iron in perovskite until pressures that far exceed those of the lower mantle, although they could still occur in ferric iron.

Here we study spin transitions of iron in perovskite using *ab initio* calculations. In conjunction with results from our previous work [8,19] we establish a mechanism, related to substitution type, able to explain most experimental observations. In addition, we show that the elastic properties of perovskite incorporating ferrous iron in a high and low-spin state are very similar, particularly at the concentrations expected in the bulk of the lower mantle. These results, taken together, eliminate the possibility that a change in the spin state of ferrous iron in lower mantle perovskite could result in an observable seismic discontinuity.

2. Computational details

It is well-known that standard density functional methods can fail to predict the correct band structure of strongly correlated systems [20,21]. This has motivated the development of new methods, such as LDA+U [22], self-interaction correction [23] and the use of hybrid functionals [20]. Despite the availability of these techniques it is not possible to know *a priori* when standard density functional theory will fail, or which of these methods is the most suitable for a particular problem. For instance, standard density functional theory predicts iron oxide to be a metal [20,24] when it is known to be an insulator, and while using self-interaction correction methods [25,26], LDA+U [27,28] and hybrid functional methods [20] all correct for this, they do not give the same physical description of band gap formation. In addition, even though standard density functional theory calculations determine the wrong band structure, they do predict equation-of-state parameters well [24,29]. It is often assumed, therefore, as it is here, that standard density functional methods may be used to calculate other properties of transition metal oxides such as magnetic state, lattice parameters and elastic moduli [7,8,19,30].

Experimental investigations have shown that lower mantle perovskite is expected to have a ferrous iron to magnesium ratio of about 6% [1]. Though debate exists over the precise crystallographic location of iron in perovskite in the lower mantle, it is thought that both ferrous and ferric iron substitute into the pseudo-dodecahedral magnesium site, with ferric iron being charge-balanced by aluminum in the octahedral silicon site [31,32]. In earlier studies we investigated the spin state of ferric iron incorporated into magnesium silicate perovskite via charge coupled substitution with aluminum [19]. Here we broaden our investigation to include ferrous iron substituting for magnesium, and ferric iron incorporated via a double charge coupled substitution (*i.e.* with ferric iron substituting into a magnesium and silicon site.) For this, a similar eighty atom magnesium silicate perovskite model was fabricated, but with a single magnesium atom substituted by ferrous iron. In addition to this, eight models: five containing two ferrous iron substitutions and three containing two ferric iron substitutions were also fashioned. The specific details of these substitutions and the names to which the models will subsequently be referred are listed in Table 1.

Simulations were performed using the projector-augmented-wave implementation [33,34] of the density functional theory based VASP simulation code [35,36].

Table 1
Initial fractional coordinates and separation of iron substitutions in iron bearing $MgSiO_3$ perovskite models at 80 GPa

Model	Fe_{Mg} ($Mg^{2+}\rightarrow Fe^{2+}$)	$Fe_{Mg'}$ ($Mg^{2+}\rightarrow Fe^{2+}$)	$d(Fe_{Mg}–Fe_{Mg'})$/Å
SSM1	(0.49, 0.04, 0.25)	(0.26, 0.29, 0.25)	3.12
SSM2	(0.74, 0.21, 0.75)	(0.26, 0.29, 0.25)	5.42
SSM3	(0.26, 0.79, 0.25)	(0.26, 0.29, 0.25)	4.68
SSM4	(0.51, 0.46, 0.75)	(0.26, 0.29, 0.25)	4.27
SSM5	(0.24, 0.21, 0.75)	(0.26, 0.29, 0.25)	3.30

Model	Fe_{Mg} ($Mg^{2+}\rightarrow Fe^{3+}$)	Fe_{Si} ($Si^{4+}\rightarrow Fe^{3+}$)	$d(Fe_{Mg}–Fe_{Si})$/Å
CCM1	(0.51, 0.46, 0.75)	(0.50, 0.25, 0.50)	2.58
CCM3	(0.49, 0.54, 0.25)	(0.50, 0.25, 0.50)	3.12
CCM5	(0.01, 0.96, 0.75)	(0.50, 0.25, 0.50)	5.47

The exchange-correlation functional used adhered to the PW91 form of the generalized gradient approximation [37,38], although a number of calculations using the local density approximation [39,40] were also performed for comparison reasons. Unless otherwise stated all following results correspond to calculations using the generalized gradient approximation. Each model was optimized with the iron ions in selected spin states, at various pressures in the range 40–160 GPa, using a plane–wave cut-off of 1000 eV and a $2\times2\times2$ Monkhorst–Pack grid [41]. This ensured that enthalpy differences were converged to 0.05 meV/atom. The calculated band structure for each model was of a metallic nature. To determine athermal elastic constants three different orthorhombic and one triclinic strains, of magnitude ±0.3, ±0.7 and ±1.0% were applied to the optimized models, the induced stresses calculated and stress–strain relation fit to a second-order polynomial. For evaluating elastic constants, Brillouin zone sampling was restricted to the Γ-point. Employing a $2\times2\times2$ Monkhorst–Pack grid caused the elastic tensors to differ by an average of about half of a percent.

3. Results

The relative enthalpies for selected iron bearing perovskite models are listed in Table 2. One can see that enthalpies of the five ferrous iron containing perovskite models are very similar at a given pressure. In comparison, the enthalpies of those that incorporate ferric iron differ by 0.44 eV. This is probably because the charge coupled substitution of ferric iron into the magnesium and silicon sites results in an unfavorable separation of charge, with the energy of the system strongly dependent on the relative distance between them; this is minimized when they are closest to each other.

Table 2
Calculated preferred spin state and enthalpy for each $Mg_{0.8750}Fe_{0.1250}SiO_3$ model at selected pressures

	80 GPa			160 GPa		
	Spin state		H/eV	Spin state		H/eV
	Fe_{Mg}	$Fe_{Mg'}$		Fe_{Mg}	$Fe_{Mg'}$	
SSM1	4/2	−4/2	−269.49	0/2	0/2	−17.43
SSM2	4/2	−4/2	−269.48	0/2	0/2	−17.20
SSM3	4/2	−4/2	−269.48	0/2	0/2	−17.32
SSM4	4/2	−4/2	−269.47	0/2	0/2	−17.48
SSM5	4/2	−4/2	−269.52	0/2	0/2	−17.49
	80 GPa			120 GPa		
	Spin state		H/eV	Spin state		H/eV
	Fe_{Mg}	Fe_{Si}		Fe_{Mg}	Fe_{Si}	
CCM1	1/2	−1/2	−265.87	1/2	−1/2	–
CCM3	5/2	−1/2	−265.58	5/2	−1/2	−135.29
CCM5	5/2	−1/2	−265.43	5/2	−1/2	−135.09

Table 3
Calculated spin transitions and their corresponding pressures for ferrous and ferric iron in perovskite

	Spin transition					P (GPa)
	Fe_{Mg}	$Fe_{Mg'/Si}$	→	Fe_{Mg}	$Fe_{Mg'/Si}$	
$Mg_{0.9375}Fe_{0.0625}SiO_3$						
	4/2	–	→	0/2	–	146
$Mg_{0.8750}Fe_{0.1250}SiO_3$ [LDA values in parenthesis]						
SSM1	4/2	−4/2	→	0/2	0/2	128 [76]
SSM2	4/2	−4/2	→	0/2	0/2	139 [93]
SSM3	4/2	−4/2	→	0/2	0/2	136 [86]
SSM4	4/2	−4/2	→	0/2	0/2	143
SSM5	4/2	−4/2	→	0/2	0/2	127
$(Mg_{0.9375}Fe_{0.0625})(Si_{0.9375}Fe_{0.0625})O_3$						
CCM1	5/2	−1/2	→	1/2	−1/2	61
CCM3	5/2	−1/2	→	1/2	−1/2	131
CCM5	5/2	−1/2	→	1/2	−1/2	148
$(Mg_{0.9375}Fe_{0.0625})(Al_{0.0625}Si_{0.9375})O_3$ [a]						
CCM1	5/2	–	→	1/2	–	105
CCM2	5/2	–	→	1/2	–	133
CCM3	5/2	–	→	1/2	–	125
CCM4	5/2	–	→	1/2	–	130
CCM5	5/2	–	→	1/2	–	125
$FeSiO_3$						
	4/2	−4/2	→	0/2	0/2	284

[a] Take from Li et al. [19].

Calculated high to low-spin transition pressures for ferrous and ferric iron in magnesium silicate perovskite are listed in Table 3, with those determined in earlier work for ferric iron in alumina-bearing magnesium silicate perovskite [19] also presented for comparison. The highest spin transition pressures are those of ferrous iron located in magnesium sites, with a range of about 130–145 GPa; within this range the lowest correspond to configurations where the cations are closest together, which are also the most favorable. Ferric iron located in magnesium sites, charge-coupled with aluminum has a lower spin transition range of 105–130 GPa, which goes down to 60–150 GPa when charge-coupled with another ferric iron, as seen in other recent calculations [16]. Ferric iron in silicon sites was found to be in a low-spin state at all pressures, in accord with earlier theoretical results [19]. Intermediate spin states were also found to be unfavorable at all times. While this too agrees with previous theoretical results [19], it is at odds

with suggestions of partial spin pairing, based on experimental work [11].

It is important to note that, the generalized gradient approximation, used in this work, is well known to overestimate cell volumes and consequently calculated equations-of-state often need to be shifted to lower pressures to be brought into good agreement with experimental results. If we assume that spin transitions are predominantly induced by constriction of *d* orbitals, as the volume per atom decreases, it follows that spin transition pressures will also be overestimated. In addition, static calculations, such as were performed, neglect the effect of zero point motion and thermal motion. To try to account for these differences, between our results and experiment, the SSM1 model was optimized with its volume fixed at that determined, at 0 GPa and 300 K, for a $Mg_{0.88}Fe_{0.12}SiO_3$ perovskite, from experiment [42]. The calculated isostatic pressure on the cell at this volume was about 7.6 GPa. This is a reasonable first-order approximation of the degree to which our calculated spin transition pressures are overestimated as a result of using the generalized gradient approximation and neglecting zero point and thermal motion. If this pressure is subtracted from our calculated spin transition pressures it brings them into better agreement with experimental observations [10,11].

For comparison, the local density approximation was also used to calculate the spin transition pressures of iron in several of the simple substitution models. These were found to be about 50 GPa lower than when using the generalized gradient approximation. This is partly due to the fact that, opposite to the generalized gradient approximation, the local density approximation generally underestimates cell volumes and, therefore, underestimates pressures, but it is principally a consequence of LDA underestimating magnetic stabilization energies [29,43]. It is expected that LDA+U calculations will give spin transition pressures higher than standard local density approximation calculations, and probably similar to those that we have determined using the generalized gradient approximation.

Previous work looking at ferric iron charge-coupled substituted with aluminum, showed that imposing a shear strain of 1% on a cell, can cause spin transition pressures to decrease by up to 15 GPa [19]. Similar decreases, of about 20 GPa were also observed for the simple substitution models.

4. Discussion

Badro et al. [10] reported that, in their experimental work, two distinct electronic spin transitions were observed for iron incorporated in perovskite, with about half of the spin on the iron atoms being lost at 70 GPa and the other half at 120 GPa. In fact, the sharpness of the first transition was not well constrained, and their data is more or less consistent with the results of Li et al. [11], who noted a gradual loss of about half of the spin on the iron atoms by 100 GPa. More recent work of Jackson et al. [15], suggested that the loss of spin originating from ferric iron in perovskite specifically is continuous and complete by around 70 GPa, in better agreement with Badro et al. [10]. Note that, neither of the latter two studies achieved the pressures required to observe the higher-pressure transition reported by Badro et al. [10]. Our results are consistent with a gradual loss of spin up to 120 GPa due to transitions in ferric iron, and a sharp loss of spin just above 120 GPa due to transitions in ferrous iron, depending on sample preparation and treatment.

The results of two of the experimental investigations [11,15] suggest that iron in perovskite begins to loose spin at pressures as low as 20 GPa. The lowest spin transition pressure we have calculated is about 60 GPa, for ferric iron in the CCM1 substitution configuration. One explanation for this is that in these studies the experimental samples experienced some non-hydrostatic stresses, since shear stresses as little as 1% are calculated to lower spin transitions by as much as 20 GPa. It is also possible that at low pressures, the observed shift in the satellite peak of the X-ray emission spectra occurs not due to spin transitions, but a decrease in magnetic moment as the *d* orbitals are compressed.

Based on Mössbauer analysis, Jackson et al. [15] suggested that spin transitions associated with ferric iron in perovskite are complete by around 70 GPa, This is much lower than the 100 GPa at which spin is still being lost in the work of Li et al. [11], and also lower than the two highest calculated spin transitions pressures, associated with the CCM3 and CCM5 substitution configurations. One explanation for this is that in the samples of Jackson et al. [15] most ferric iron was in the CCM1 arrangement. This is not an unreasonable assumption since it is more stable than the others, seen in Table 2. The samples studied by Li et al. [11], on the other hand, could have contained ferric iron in the CCM3 and CCM5 substitutions configurations, with their calculated spin transition pressures lowered to observed values, as a result of non-hydrostatic stresses. Given that substitution configuration has a significant effect on the spin transition pressure of ferric iron, leading to a wide range of values between 60–150 GPa, it may be that the experimental samples of Li et al. [11] simply contained iron in a greater range of substitution configurations

(including ones which we did not consider here), and these led to a wider range of transition pressures, which appeared as continuous. It is not clear, however, why the samples from the two sets of experiments would have different arrangements of ferric iron, but it may have to do with subtle differences in their preparation and treatment.

In the case of ferrous iron, our results suggest that substitution configuration has a small effect on spin transition pressure, leading to a narrow range of values between 130–145 GPa. The sharp spin transition observed at 120 GPa by Badro et al. [10], can, therefore, be associated with spin loss from ferrous iron, as has been suggested [17]. This would not be observed in other studies [11,15], because they did not subject samples to such high pressures, and could also explain why in one investigation iron was still observed to exhibit some spin at 100 GPa [11].

It is observed that, at a given pressure, iron in alumina-bearing perovskite exhibits a higher spin than alumina-free [11]. This can be explained by the fact that ferric iron in silicon sites is calculated to be in a low-spin state at all pressures. It has been shown that in alumina-bearing perovskite, ferric iron is predominantly located in magnesium sites, charge-balanced by aluminum in silicon sites [31,32]. In alumina-free perovskite, however, ferric iron in magnesium sites must be charge-balanced by ferric iron in silicon sites, which will always be in a low-spin state. Since 40% of iron in alumina-free perovskite is expected to be ferric [15], 20% of the total iron will be in a low-spin state, even at zero pressure. Presuming that both perovskites studied by Li et al. [11] contained similar amounts of ferric iron, this explains why iron in the alumina-bearing sample was observed to have a higher average spin than that in the alumina-free sample. In addition, since ferric iron charge-coupled substituted with aluminum has a higher spin transition pressure than that charge-coupled substituted with ferric iron, ferric iron in alumina-bearing perovskite will retain spin up to higher pressures.

It is, of course, important to understand how the high temperatures of the lower mantle would affect the calculated spin transitions pressures. This is difficult due to the lack of relevant data. Original estimates of an increase of 15–18 GPa [10,17] have been suggested to be low [18], due to an overestimation in the volume change when going from high to low-spin. It has been proposed instead that, at lower mantle temperatures, ferrous iron in perovskite will only reach a stable low-spin state above 200 GPa [18], which far exceeds pressures of the deep Earth. On the other hand, ferric iron, in perovskite, is postulated to undergo partial conversion to a low-spin state at lower mantle conditions [18], as is ferrous iron in magnesiowüstite.

If we take the lowest estimate, and assume that at lower mantle temperatures our calculated spin transition pressures will be only 15 GPa higher [17], those of ferrous iron become almost too high to occur in the Earth, even with our calculated correction factor. Note that, they also exceed the calculated perovskite to post-perovskite phase transition pressure for a ferrous iron-bearing phase [44], with ferrous iron expected to be in a high-spin state in post-perovskite throughout the lower mantle [45]. In the case of ferric iron, only the spin transition associated with the CCM1 substitution configuration is plausible at high temperatures, and as it is the most energetically favorable, one could expect the majority of ferric iron to adopt the arrangement. In addition, although ferric iron is expected to substitute into magnesium sites, charge-balanced by aluminum in

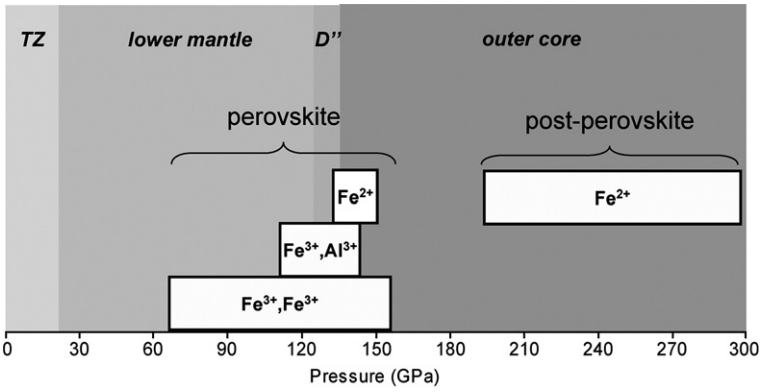

Fig. 1. Estimated spin transition pressure ranges for iron in perovskite and post-perovskite at 2500 K, assuming that the only effect of temperature is to increase values by 15 GPa, as estimated for iron in perovskite at 120 GPa by Badro et al. [17]. Spin transition pressures for post-perovskite, taken from Stackhouse et al. [45], are also shown with the same effect of temperature assumed.

Table 4
Calculated density and athermal elastic moduli of iron-bearing $MgSiO_3$ perovskite (in GPa)

P (GPa)	Spin state		ρ (kg m^{-3})	C_{11}	C_{22}	C_{33}	C_{12}	C_{13}	C_{23}	C_{44}	C_{55}	C_{66}	K_T	G_T
	Fe_{Mg}	$Fe_{Mg'}$												
$MgSiO_3$ [a]														
40	–	–	4543	629	741	679	245	229	237	247	207	211	385	221
136	–	–	5454	955	1239	1186	562	448	472	376	277	369	699	326
$Mg_{0.9375}Fe_{0.0625}SiO_3$														
136	0/2	–	5555	968	1237	1191	575	447	471	369	278	354	704	322
136	4/2	–	5543	965	1233	1189	573	443	473	375	277	352	703	323
$Mg_{0.8750}Fe_{0.1250}SiO_3$ — *SSM1 model*														
40	0/2	0/2	4726	633	736	679	265	222	240	238	209	210	388	219
40	4/2	−4/2	4704	631	730	679	259	220	245	244	205	204	387	218
40	4/2	4/2	4703	631	730	679	259	221	245	245	205	204	387	218
136	0/2	0/2	5657	976	1233	1192	582	452	475	362	274	349	709	319
136	4/2	−4/2	5635	969	1225	1186	577	446	480	370	272	343	705	318
136	4/2	4/2	5635	969	1224	1186	576	446	481	370	273	342	705	318
$Mg_{0.8750}Fe_{0.1250}SiO_3$ — *SSM2 model*														
136	0/2	0/2	5657	977	1231	1190	580	453	475	354	274	348	709	316
136	4/2	−4/2	5635	970	1224	1187	578	446	480	369	273	342	705	318
136	4/2	4/2	5634	970	1224	1187	577	446	481	369	273	344	705	318
$FeSiO_3$ [b]														
136	4/2	−4/2	6898	1036	1120	1165	600	494	552	324	227	263	732	272

[a] Taken from Stackhouse et al. [47].
[b] Taken from Stackhouse et al. [44].

silicon sites [31,32], our previous theoretical investigations [19] indicate that, this is only true at relatively low pressures, and at those expected in the deepest mantle ferric iron and aluminum are equally comfortable in both sites. This implies that more ferric iron will be present in silicon sites in the deep Earth, where it will be in a low-spin state. In the lower mantle, therefore, ferrous iron in perovskite will most probably be in a high-spin state, while the majority of ferric iron will undergo a transition to a low-spin state at mid-to-deep mantle pressures. Since up to 50% of iron in perovskite is estimated to be ferric [46], this spin transition could have a quite significant effect on mantle convection [10,13]. Fig. 1 illustrates the predicted spin transition pressures ranges for iron in perovskite and post-perovskite at 2500 K, assuming that the only effect of temperature is to increase values by 15 GPa, as estimated for iron in perovskite at 120 GPa by Badro et al. [17]. Spin transition pressures for post-perovskite, taken from Stackhouse et al. [45], are also shown with the same effect of temperature assumed.

Elastic constants calculated for selected perovskite models are reported in Table 4. Incorporation of iron into $MgSiO_3$ perovskite produces an expected increase in density, a larger bulk modulus and lower shear modulus. This is in agreement with observations from the pure end-members [44]. In Fig. 2 one can see how the compressional (V_P), shear (V_S) and bulk (V_Φ) isotropic wave velocities of perovskite vary as a function of ferrous iron content. Solid lines represent values

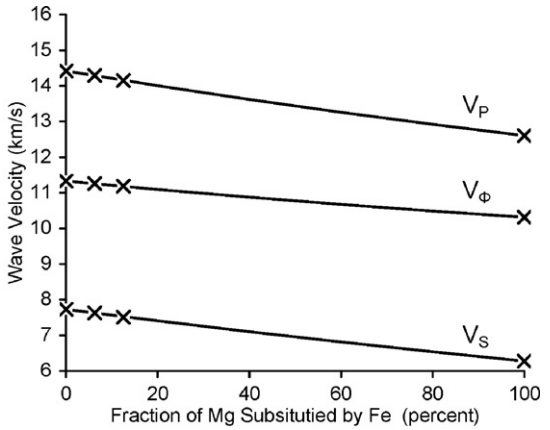

Fig. 2. Decrease in compressional (V_P), shear (V_S) and bulk (V_Φ) isotropic wave velocities for perovskite as a function of ferrous iron content at 136 GP and 0 K. Solid lines represent values calculated from linear mixing of pure end-member properties, taken from Stackhouse et al. [44,47], while markers show values determined for models incorporating explicit percentages of iron.

Table 5
Derivatives of density, bulk and shear moduli and seismic velocities of (Mg, Fe)SiO_3 perovskite with respect to iron content

	P (GPa)	T (K)	$\partial\ln\rho/\partial$Fe	$\partial\ln K_T/\partial$Fe	$\partial\ln G_T/\partial$Fe	$\partial\ln V_P/\partial$Fe	$\partial\ln V_S/\partial$Fe	$\partial\ln V_\Phi/\partial$Fe
This work	136	0	−0.2334	−0.0461	−0.1819	−0.1341	−0.2076	−0.0936
This work	40	0	−0.2781	−0.0435	−0.1410	−0.1571	−0.2095	−0.1173
Kiefer et al., 2002 [a]	0	0	−0.2744	−0.0753	−0.2313	−0.1718	−0.2528	−0.0995

[a] Local density approximation used.

calculated from linear mixing of densities, bulk and shear moduli of pure end-members, taken from previous studies [44,47], while markers show values for models incorporating the explicit percentages of iron from the present work. One can see that, linear mixing of the properties of pure end-members provides a good estimate of the isotropic wave velocities of intermediate compositions. Logarithmic derivatives of the elastic and seismic properties of perovskite as a function of ferrous iron content are presented in Table 5. These are, in general, similar in magnitude to those reported for the post-perovskite phase [45], except that the shear modulus of perovskite decreases about 30% less with ferrous iron content, due to the smaller effect it has on the C_{44} elastic tensor. The results also compare well with values deduced from the results of previous calculations on iron-bearing perovskite [7].

When incorporated in the low amounts considered in this work, the spin state of ferrous iron has a small effect on the elastic properties of perovskite, with bulk and shear moduli increasing by about half a percent upon a high to low-spin transition at 136 GPa. This is similar to observations for ferric iron in perovskite [8] and ferrous iron in post-perovskite [45], but in contrast to those for ferrous iron in magnesiowüstite, where a high to low-spin transition is seen to have a large effect on bulk modulus [9]. Fig. 3 illustrates how the volume difference for perovskite containing ferrous iron in a high and low-spin state increases with iron content, but decreases with pressure. In view of this, the discrepancies could be attributed to differences in iron content and pressure. Note that for any iron to magnesium ratio the volume fraction of iron in magnesiowüstite is two and a half times that of perovskite or post-perovskite, due to their different formula units. In addition, the bulk modulus of magnesiowüstite was contrasted at 60 GPa [9], whereas we compare elastic properties at 136 GPa. Elastic constants determined for the SSM1 model at 40 GPa indicate, however, that even at low pressures the difference in elastic properties when ferrous iron is in a high and low-spin state is small.

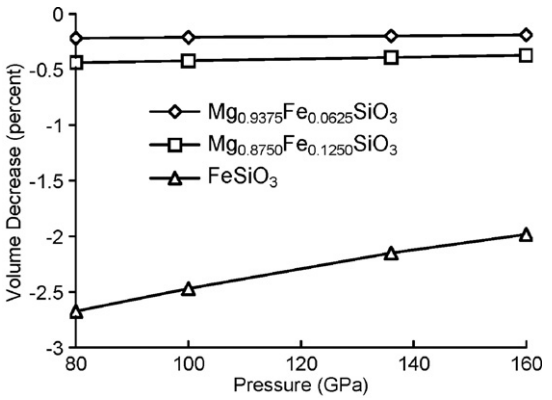

Fig. 3. Difference in volume for perovskite containing ferrous iron in a high and low-spin state at 0 K, as a function of composition and pressure. The $FeSiO_3$ values are taken from Stackhouse et al. [44].

5. Conclusions

In conclusion, our *ab initio* calculations suggest that spin transition pressures of iron in perovskite increase in the following order: ferric iron charge-coupled substituted with ferric iron, ferric iron charge-coupled substituted with aluminum, and finally ferrous iron. Substitution configuration has a large effect on the spin transition pressure of ferric iron, with the lowest values being associated with arrangements where iron substitutions are close together; these are also the most favorable. It is expected that, for the most part, ferrous iron will be in a high-spin state in the lower mantle, while ferric iron will undergo conversion to a low-spin state at mid-to-deep mantle pressures. The spin state of incorporated ferric [8] and ferrous iron has little effect on the elastic properties of perovskite, in contrast with the large effect it has on those of magnesiowüstite [9].

Acknowledgements

This work is funded by the NERC sponsored Deep Earth System consortium grant no. NER/O/S/2001/01262. The calculations were run on machines maintained by the HPCx consortium and University College London research computing services.

References

[1] K.K.M. Lee, B. O'Neill, W.R. Panero, S.-H. Shim, L.R. Benedetti, R. Jeanloz, Equation of state of the high-pressure phases of a natural peridotite and implications for the Earth's lower mantle, Earth Planet. Sci. Lett. 223 (2004) 381–393.

[2] M. Murakami, K. Hirose, K. Kawamura, N. Sata, Y. Ohishi, Post-perovskite phase transition and mineral chemistry in the pyrolitic lowermost mante, Geophys. Res. Lett. 32 (2005) L03304.

[3] E.J. Garnero, D.V. Helmberger, A very low basal layer underlying large-scale low-velocity anomalies in the lower mantle beneath the Pacific: evidence from core phases, Phys. Earth Planet. Inter. 91 (1995) 161–176.

[4] D.P. Dobson, J.P. Brodholt, Subducted banded iron formations as a source of ultralow-velocity zones at the core–mantle boundary, Nature 434 (2005) 371–374.

[5] S. Rost, E.J. Garnero, Q. Williams, M. Manga, Seismological constraints on a possible plume root at the core–mantle boundary, Nature 435 (2005) 666–669.

[6] W.L. Mao, H.-K. Mao, W. Sturhahn, J. Zhao, V.B. Prakapenka, Y. Meng, J. Shu, Y. Fei, R.J. Hemley, Iron-rich post-perovskite and the origin of ultralow-velocity zones, Science 312 (2006) 564–565.

[7] B. Kiefer, L. Stixrude, R.M. Wentzcovitch, Elasticity of (Mg, Fe) SiO_3-perovskite at high pressures, Geophys. Res. Lett. 29 (2002) L014683.

[8] L. Li, J.P. Brodholt, S. Stackhouse, D. Weidner, M. Alfredsson, G.D. Price, Elasticity of (Mg, Fe)(Si, Al)O_3-perovskite at high pressure, Earth Planet. Sci. Lett. 240 (2005) 529–536.

[9] J.-F. Lin, V.V. Struzhkin, S.D. Jacobson, M.Y. Hu, P. Chow, J. Kung, H. Liu, H.-K. Mao, R.J. Hemley, Spin transition of iron in magnesiowüstite in the Earth's lower mantle, Nature 436 (2005) 377–380.

[10] J. Badro, J.-P. Rueff, G. Vankó, G. Monaco, G. Fiquet, F. Guyot, Electronic transitions in perovskite: possible nonconvecting layers in the lower mantle, Science 305 (2004) 383–386.

[11] J. Li, V.V. Struzhkin, H.-W. Mao, J. Shu, R.J. Hemley, Y. Fei, B. Mysen, P. Dera, V. Prakapenka, G. Shen, Electronic spin state of iron in lower mantle perovskite, Proc. Natl. Acad. Sci. 101 (2004) 14027–14030.

[12] J. Badro, G. Fiquet, F. Guyot, J.-P. Rueff, V.V. Struzhkin, G. Vankó, G. Monaco, Iron partitioning in Earth's mantle: toward a deep lower mantle discontinuity, Science 300 (2003) 789–791.

[13] A.F. Goncharov, V.V. Struzhkin, S.D. Jacobson, Reduced radiative conductivity of low-spin (Mg, Fe)O in the lower mantle, Science 312 (2006) 1205–1208.

[14] W. Sturhahn, J.M. Jackson, J.-F. Lin, The spin state of iron in minerals of Earth's lower mantle, Geophys. Res. Lett. 32 (2005) L12307.

[15] J.M. Jackson, W. Sturhahn, G. Shen, J. Zhao, M.Y. Hu, D. Errandonea, J.D. Bass, Y. Fei, A Synchrotron Mössbauer Spectroscopy study of (Mg,Fe)SiO_3 perovskite up to 120 GPa, Am. Mineral. 90 (2005) 199–205.

[16] F. Zhang, A.R. Oganov, Valence state and spin transitions of iron in Earth's mantle silicates, Earth Planet. Sci. Lett. 249 (2006) 436–443.

[17] J. Badro, G. Fiquet, F. Guyot, Thermochemical state of the lower mantle: new insights from mineral physics, in: R.D. van der Hilst, J.D. Bass, J. Matas, J. Trampert (Eds.), Earth's Deep Mantle: Structure, Composition and Evolution, Geophysical Monograph, vol. 160, American Geophysical Union, Washington D. C, 2005, pp. 241–260.

[18] A.M. Hofmeister, Is low-spin Fe^{2+} present in Earth's mantle? Earth Planet. Sci. Lett. 243 (2006) 44–52.

[19] L. Li, J.P. Brodholt, S. Stackhouse, D. Weidner, M. Alfredsson, G.D. Price, Electronic spin state of ferric iron in al-nearing perovskite in the lower mantle, Geophys. Res. Lett. 32 (2005) L17307.

[20] M. Alfredsson, G.D. Price, C.R.A. Catlow, S.C. Parker, R. Orlando, J.P. Brodholt, Electronic structure of the antiferromagnetic *B1*-structured FeO, Phys. Rev., B 70 (2004) 165111.

[21] M. Cococcioni, S. Dal Corso, S. de Gironcoli, Structural, electronic and magnetic properties of Fe_2SiO_4 fayalite: comparison of LDA and GGA results, Phys. Rev., B 67 (2003) 094106.

[22] V.I. Anisimov, J. Zaanen, O.K. Andersen, Band theory of Mott insulators: Hubbard U instead of Stoner I, Phys. Rev., B 44 (1991) 943–954.

[23] A. Svane, W.M. Temmerman, Z. Szotek, J. Lægsgaard, H. Winter, Self-intercation-corrected local-spin-density calculations for rare earth metals, Int.J. Quantum. Chem. 77 (2000) 799–813.

[24] D.G. Isaak, R.E. Cohen, M.J. Mehl, D.J. Singh, Phase stability of wüstite at high pressure from first-principles linearized augmented plane–wave calculations, Phys. Rev., B 47 (1993) 7720–7731.

[25] A. Svane, O. Gunnarsson, Transition-metal oxides in the self-interaction-corrected density-functional formalism, Phys. Rev. Lett. 65 (1990) 1148–1151.

[26] Z. Szotek, W.M. Temmerman, H. Winter, Application of the self-interaction correction to transition-metal oxides, Phys. Rev., B 47 (1993) 4029–4032.

[27] I.I. Mazin, V.I. Anisimov, Insulating gap in FeO: correlations and covalency, Phys. Rev., B 55 (1997) 12822–12825.

[28] S.A. Gramsch, R.E. Cohen, S.Y. Savrasov, Structure, metal-insulator transitions, and magnetic properties of FeO at high pressures, Am. Mineral. 88 (2003) 257–261.

[29] R.E. Cohen, I.I. Mazin, D.G. Isaak, Magnetic collapse in transition metal oxides at high pressure: implication for the Earth, Science 275 (1997) 654–657.

[30] R. Caracas, R.E. Cohen, Effect of chemistry on the stability and elasticity of the perovskite and post-perovskite phases in the $MgSiO_3$–$FeSiO_3$–Al_2O_3 system and implications for the lowermost mantle, Geophys. Res. Lett. 32 (2005) L16310.

[31] N.C. Richmond, J.P. Brodholt, Calculated role of aluminum in the incorporation of ferric iron into magnesium silicate perovskite, Am. Mineral. 83 (1998) 947–951.

[32] C.B. Vanpeteghem, R.J. Angel, N.L. Ross, S.D. Jacobsen, D.P. Dobson, K.D. Litasov, E. Ohtani, Al, Fe, substitution in the $MgSiO_3$ perovskite structure: a single-crystal X-ray diffraction study, Phys. Earth Planet. Inter. 155 (2006) 96–103.

[33] P.R. Blöchl, Projector augmented-wave method, Phys. Rev., B 50 (1994) 17953–17979.

[34] G. Kresse, D. Joubert, From ultrasoft pseudopotentials to the projector augmented-wave method, Phys. Rev., B 59 (1999) 1758–1775.

[35] G. Kresse, J. Furthmüller, Efficient interative schemes for ab initio total-energy calculations using a plane–wave basis set, Phys. Rev., B 54 (1996) 11169–11186.

[36] G. Kresse, J. Furthmüller, Efficiency of ab initio total energy calculations for metals and semiconductors using a plane–wave basis set, Comput. Mater. Sci. 6 (1996) 15–50.

[37] Y. Wang, J.P. Perdew, Correlation hole of the spin-polarized electron-gas, with exact small-wave-vector and high density scaling, Phys. Rev., B 44 (1991) 13298–13307.

[38] J.P. Perdew, J.A. Chevary, S.H. Vosko, K.A. Jackson, M.R. Pederson, D.J. Singh, C. Fiolhais, Atoms, molecules, solids, and

surfaces — applications of the generalized gradient approximation for exchange and correlation, Phys. Rev., B 46 (1992) 6671–6687.
[39] D.M. Ceperley, B.J. Alder, Ground state of the electron gas by a stochastic method, Phys. Rev. Lett. 45 (1980) 566–569.
[40] J.P. Perdew, A. Zunger, Self-interaction correction to density-functional approximations for many-electron systems, Phys. Rev., B 23 (1981) 5048–5079.
[41] H.J. Monkhorst, J.D. Pack, Special points for Brillouin-zone integrations, Phys. Rev., B 13 (1976) 5188–5192.
[42] E. Knittle, R. Jeanloz, Synthesis and equation of state of (Mg, Fe) SiO3 perovskite to over 100 gigapascals, Science 235 (1987) 668–670.
[43] L. Stixrude, R.E. Cohen, D.J. Singh, Iron at high pressure: linearized-augmented-plane–wave computations in the generalized-gradient approximation, Phys. Rev., B 50 (1994) 6442–6445.
[44] S. Stackhouse, J.P. Brodholt, G.D. Price, Elastic anisotropy of $FeSiO_3$ end-members of perovskite and post-perovskite phases, Geophys. Res. Lett. 33 (2006) L01304.
[45] S. Stackhouse, J.P. Brodholt, D.P. Dobson, G.D. Price, Electronic spin transitions and the seismic properties of ferrous iron-bearing post-perovskite, Geophys. Res. Lett. 33 (2006) L12S03.
[46] C. McCammon, Perovskite as a possible sink for ferric iron in the lower mantle, Nature 387 (1997) 694–696.
[47] S. Stackhouse, J.P. Brodholt, G.D. Price, High temperature elastic anisotropy of the perovskite and post-perovskite polymorphs of Al_2O_3, Geophys. Res. Lett. 32 (2005) L13305.